Improved model representation of the contemporary Greenland ice sheet firn layer

Max Brils, Peter Kuipers Munneke, Willem Jan van de Berg, Michiel van den Broeke

Institute for Marine and Atmospheric Research, Utrecht University, Utrecht, The Netherlands

Abstract

The firn layer that covers 90% of the Greenland ice sheet (GrIS) plays an important role in determining the response of the ice sheet to climate change. Meltwater can percolate into the firn layer and refreeze at colder depths, temporarily preventing mass loss. However, as global warming leads to an increase in melt, this buffer capacity may be disappear, leading to a tipping point in meltwater runoff. It is therefore important to study the evolution of the Greenland firn layer in order to gain a deeper understanding of their climate response. In this study, we present our latest version of the Greenland version of our dedicated firn model, IMAU-FDM. Through the use of recently published parameterizations and observations of firn density, temperature and liquid water content at the Greenland ice sheet, changes have been made to the freshly fallen snow density, the dry snow densification rate and the firn's thermal conductivity. The new model settings lead to overall higher firn air content and higher temperatures at 10 m deep owing to a lower density near the surface. The effect of the new model settings on the elevation is investigated through three case studies located at Summit, KAN-U and FA-13. Most notably, the updated model shows greater inter- and intra-annual variability in elevation and an increase in sensitivity to its climate forcing. This is mainly caused by an increase in the dry snow densification rate in combination with a lower surface density.

Keywords: climate change, ice/atmosphere interactions, polar firn, snow/ice surface processes, firn modelling, elevation change

1. Introduction

Firn, the layer of compressed snow that represents the transitional product between seasonal snow and ice in the accumulation zone of glaciers, strongly influences the climate response of mountain glaciers, ice caps and ice sheets. Pore space between snow grains that make up the firn layer enable meltwater to percolate into, and refreeze – in the firn layer if temperatures are below freezing. This prevents runoff. It has been demonstrated that refreezing is a critical process for many ice caps to survive, e.g. in the Canadian Arctic. On these ice caps, summer melt consistently exceeds annual snowfall, and refreezing is required to maintain a near-zero mass balanceNoël et al. [1]. As melt rates increase further in response to global warming, firn pore space is increasingly taken up by refrozen meltwater, degrading the efficiency of the refreezing process until at some point it collapses. This is happening to Greenland's marginal ice caps since the mid 1990s, accelerating mass loss and initiating their irreversible demise in the coming centuriesNoël et al. [2].

The saturation tipping point is not yet reached for the Greenland ice sheet (GrIS). The GrIS has a much more extensive firn layer ($\sim 1.71 \times 10^6\,\mathrm{m}^2$), which is higher in elevation (on average $\sim$2100 m above sea level (a.s.l.)) and hence more porous and colder than firn on other Arctic ice capsNoël et al. [3]. With a depth of up to 80 m Kuipers Munneke et al. [4], Vandecrux et al. [5] estimated that the GrIS firn layer contains a total of $(26\,800 \pm 1840)\,\mathrm{km}^3$ of air. This is equivalent to more than 60 times the total annual 1961-1990 average volume of GrIS meltwater productionVan Den Broeke et al. [6], although this reduces to a factor of $\sim 1-4$ if only pore space in the percolation zone is considered (Harper et al. [7]). Model estimates show that for the same period, no less than 44 % of the meltwater produced at the surface of the GrIS refroze in the firn layerVan Den Broeke et al. [6], Mouginot et al. [8].

Surface melt is also increasing in the GrIS accumulation zone, with the extreme melt summers of 2012 and 2019 as vivid examples (Nghiem et al. [9], Sasgen et al. [10]). These high-melt summers also led to peaks in refreezing, warming and densification of the firn layer (Steger et al. [11]). In some places, 1-2 m thick ice slabs are formed that prevent meltwater from reaching the pore space below (Machguth et al. [12], MacFerrin et al. [13]).

Diagnosing the current state of the GrIS firn layer, and predicting its future, is evidently important. Firn density models can be used to interpolate between the relatively sparse observations from firn cores and snow pitsKuipers Munneke et al. [4], Vandecrux et al. [5]. Another important application of modelled firn depth changes is the conversion of remotely sensed elevation (volume) changes to mass changesZwally et al. [14], Wouters et al. [15], Shepherd et al. [16]. Some (regional) climate models are interactively coupled to a snow/firn model, but these often use simplified initialization, parametrizations and/or reduced vertical resolution for computational efficiency. The main advantage of using a dedicated, offline firn densification model is the lower computational cost, which enables the use of higher vertical resolution, a proper initialization of the firn layer, and extensive sensitivity testing (Lundin et al. [17], Stevens et al. [18], Vandecrux et al. [19]). The drawback of using an offline firn model is that it must be forced unidirectionally with observed and/or modelled surface temperature and surface mass fluxes (snow, rain, sublimation, drifting snow erosion).

In this study we present an updated version of the firn densification model of the Institute for Marine and Atmospheric research Utrecht (IMAU-FDM) applied to the GrIS, forced at the upper boundary by the latest three-hourly output of the polar version of the Regional Atmospheric Climate Model (RACMO2, Noël et al. [20]). It supersedes the previous model version presented by Kuipers Munneke et al. [4] and Ligtenberg et al. [21].

We use recently published parametrizations and previously existing and newly obtained observations of firn density, temperature and liquid water content from the GrIS to calibrate model parametrizations for surface (fresh snow) density, dry snow densification rate, thermal conductivity, and meltwater percolation. The updated model is subsequently used to perform case studies of contemporary firn depth variability in three climatologically distinct locations of the GrIS accumulation zone: (1) the dry and cold interior, (2) the relatively low-accumulation western percolation zone, and (3) the high-accumulation south-eastern percolation zone.

This paper is organized as follows. In Section 2 we describes a more extended set of observations, both in time and space, that allows for new parametrizations and improved calibration of IMAU-FDM for the GrIS. In Section 2.2 we show how the altered densification and heat conduction expressions (in that order) resulted in an overall improved representation of GrIS firn density, temperature and liquid water content. The three case studies are then presented in Section 4, followed in Section 5 by a summary and outlook.

2. Methods

2.1. Observations

IMAU-FDM output is evaluated using previously available and newly obtained profiles of firn density, temperature and liquid water content from the GrIS accumulation zone. The observations are from 128 different locations to ensure that the various ice facies and climate zones of the GrIS are well represented (Fig. 1). Vertical profiles of observed firn density from ice cores vary in depth from 9.6 to 150.8 m and have been drilled between 1952 and 2018 in the framework of the Program for Arctic Regional Climate Assessment (PARCA; McConnell et al. [22], Mosley-Thompson et al. [23], Hanna et al. [24], Banta and McConnell [25]), the Arctic Circle Traverses (ACT, Box et al. [26]) and the EGIG lineHarper et al. [7], Das 1 and Das 2 (e.g. from Hanna et al. [24]) and several other cores were retrieved from the SUMup data base (SUrface Mass balance and snow depth on sea ice working grouP),Koenig et al. [27], Koenig and Montgomery [28]).

Temperature observations include profiles ranging in depth between 4 and 14 m, obtained by Harper et al. [7] along a transect in the western GrIS and at the NEEM deep ice core drilling site Orsi et al. [29]. Additional firn temperature observations are from Summit, Dye-2 (Vandecrux et al. [30], KAN-U (Charalampidis et al. [31]) and FA-13 (Koenig et al. [32]). An additional 14 observations of 10 m firn temperatures are from Polashenski et al. [33].

For observations of liquid water in firn, we use observations from Dye-2 Heilig et al. [34], obtained using an upward-looking ground-penetrating radar (upGPR), which was installed and operated in the summer of 2016. The upGPR was buried ~ 4.5 m under the snow, and was capable of measuring the liquid water percolation depth, content as well as the changing distance between the instrument and the snow surface.

2.2. IMAU-FDM

For this work we use the offline IMAU-FDM, a semi-empirical firn densification model that simulates the time evolution of firn density, temperature, liquid water content and changes in surface elevation owing to variability of firn depth. The model has been extensively compared to and calibrated with observations of firn density and temperature from the ice sheets of Greenland and Antarctica (Ligtenberg et al. [35], Kuipers Munneke et al. [4], Ligtenberg et al. [21]). IMAU-FDM is forced by three-hourly output of the polar

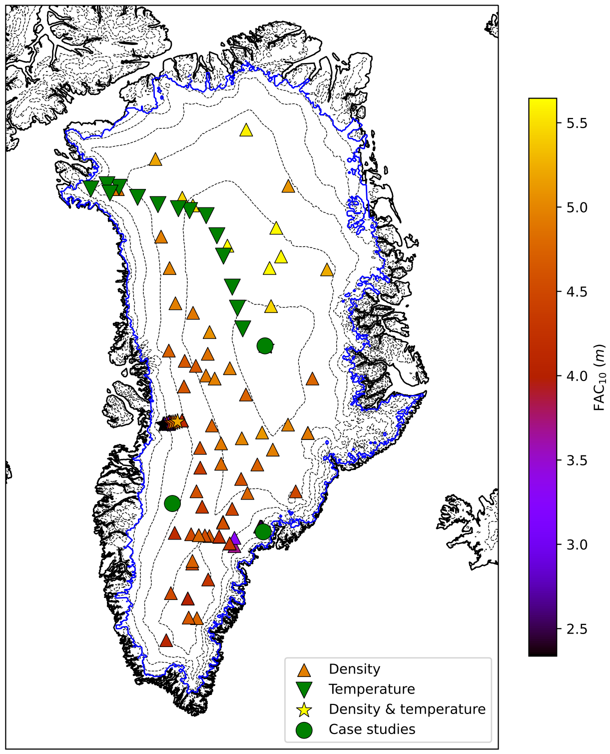

Figure 1: Locations of observed density (upward triangle), 10 m temperature (downward triangle), both (stars). The colour of the upward triangles and stars indicate the measured firn air content for the first 10 m of snow at that location (FAC_{10}). The three purple circles indicate the case studies discussed in Section 4. Dashed lines represent 500 m elevation contours, the blue solid line the contiguous ice sheet margin.

version of the Regional Atmospheric Climate Model (RACMO2.3p2). Over glaciated grid cells, the RACMO2 subsurface model uses the same expressions as IMAU-FDM, but with a lower vertical resolution (max. 150 vs. 3000 layers) and less comprehensive initialization to save computation time. In the current version of IMAU-FDM we do not consider the subsurface penetration of shortwave radiation (Van Dalum et al. [36]). For both the ice sheets of Greenland and Antarctica, the performance of IMAU-FDM has been comparable to the more physically-based SNOWPACK model (Steger et al. [37], Van Wessem et al. [38], Keenan et al. [39]). In the following subsections, we briefly describe how the main processes are currently represented in IMAU-FDM, and what improvements have been implemented compared to the previous model version.

2.2.1. Fresh snow density

An important boundary condition for the model is the density of freshly fallen snow, ρ_0. When determined from field observations, fresh snow density is often assumed equal to the near-surface density, loosely defined as the average density of the top 0.5–1 m of dry snow. As density is highly variable near the surface, the exact chosen depth is critical for the outcome, which hampers a robust comparison between datasets (Fausto et al. [40]). In firn models, fresh snow density is commonly parameterized as a function of meteorological variables such as temperature and wind speed at the time of deposition, or, when these are not available, using annual average values instead (Keenan et al. [39]). Several studies have addressed the parametrization of ρ_0 on the GrIS (Kuipers Munneke et al. [4], Fausto et al. [40]). Assuming a linear dependence of the density on mean annual surface temperature T_s, this parametrization takes on the following form:

$$\rho_0 = A + B \cdot T_s \tag{1}$$

With A and B being fitting constants and T_s in °C. In previous studies where IMAU-FDM was applied to the GrIS, $A = 481\,\mathrm{kg/m^3}$ and $B = 4.834\,\mathrm{kg/(m^3 \cdot K)}$ have been used Kuipers Munneke et al. [4], Ligtenberg et al. [21] based on observations using the 0–0.2 m average density from no-melt locations to approximate the surface value.

In the updated model, a new parameterization for fresh snow density Fausto et al. [40] was adopted. In contrast to previous studies, which typically use the first 0.5–1 m of snow, [40] used only the upper 0.1 m of snow to define surface density at 200 locations and found:

$$\rho_0 = 362.1 + 2.78 \cdot T_a \tag{2}$$

with T_a the annual mean near-surface (usually 2 m) air temperature in °C.

Previously, the climatological mean 2 m air temperature has been used in IMAU-FDM (Kuipers Munneke et al. [41]), or an instantaneous value (Ligtenberg et al. [21]). Using a climatological mean value suppresses the year-to-year variability in snow density. This is undesirable, especially if the model will be used for the modelling of possible future scenarios, in which long term trends in the temperature may have an effect. On the other hand,

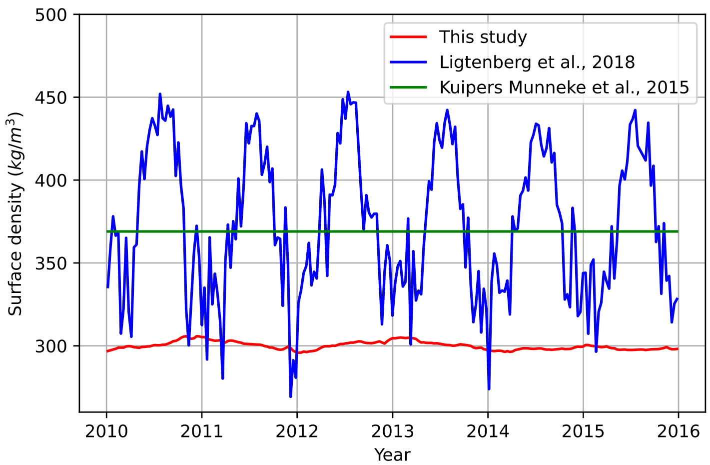

Figure 2: Daily averages of Das2 (southeast Greenland, see Fig. 1) surface density (2010-2016) using three different parametrizations.

using instantaneous temperature values may introduce an excessive variability which, in reality, is smoothened by the effects of the snow being subjected to settling by wind and metamorphosis through numerous atmospheric warming and cooling cycles. As a trade-off, in the updated model T_a is calculated as the average 2 m air temperature of the year preceding the snowfall.

Fig. 2 shows Das2 (southeast Greenland) surface density (2010-2016) from these different approaches. Clearly, temporal variations are much larger when an instantaneous T is used. Furthermore, the expression by Fausto et al. [40] results in a lower surface density overall than Kuipers Munneke et al. [41]. In subsequent sections, we refer to Ligtenberg et al. [21]) as the "old settings".

2.2.2. Dry snow densification rate

IMAU-FDM is a 1D, vertical Lagrangian model. When new snow accumulates at the surface (model top), the model layers are buried deeper and tracked during their downward motion. At every time step, each layer is compacted under the influence of the pressure exerted by the mass of snow/firn above it. However, the densification rate $\frac{\mathrm{d}\rho}{\mathrm{d}t}$ is not directly related to the overburden pressure, but rather follows a semi-empirical, temperature-dependent equation based on Arthern et al. [42]:

$$\frac{\mathrm{d}\rho}{\mathrm{d}t} = C\dot{b}g(\rho_i - \rho)e^{-\frac{E_c}{RT}+\frac{E_g}{RT}} \tag{3}$$

where $\dot{b}$ is the annual average accumulation rate (mm w.e. per year) over the spinup-period (1960-1979), $\rho_i = 917\,\mathrm{kg\,m^{-3}}$ is the adopted density of glacial ice, g, E_c, E_g and R are constants and T is the instantaneous layer temperature in Kelvin. The average annual accumulation rate $\dot{b}$ is provided by RACMO2 as the amount of total precipitation minus sublimation and drifting snow erosion. Different values of C above and below $\rho = 550\,\mathrm{kg\,m^{-3}}$ represent a shift in the dominant densification mechanism from settling to sintering (Cuffey and Paterson [43]). For $\rho < 550\,\mathrm{kg\,m^{-3}}$, the densification of the firn is dominated by the settling and sliding of grains. For $\rho >= 550\,\mathrm{kg\,m^{-3}}$ recrystallisation, deformation and sublimation become dominant and the densification rate is greater, which is reflected in a lower value for C.

Compared to observations of the depth of the 550 and 830 kg m-3 density levels, a structural bias is found, that in previous studies turned out to depend on the annual average accumulation rate. In order to calibrate Equation 3 to the new set of observations, we introduce a multiplication factor MO to better align modelled density profiles with observations:

$$\mathrm{MO} = \alpha - \beta \ln(\dot{b}) \tag{4}$$

where α and β are unitless constants. In previous studies these were $\{\alpha, \beta\} = \{1.435, 0.151\}$ for $\rho < 550\,\mathrm{kg\,m^{-3}}$ and $\{\alpha, \beta\} = \{2.366, 0.293\}$ for $\rho \geq 550\,\mathrm{kg\,m^{-3}}$ for GreenlandKuipers Munneke et al. [4]. Although the physical processes underlying the densification of firn do not explicitly depend on the accumulation rate, a correlation between $\frac{\mathrm{d}\rho}{\mathrm{d}t}$ and $\dot{b}$ may act as a proxy variable for geometric effects that are time dependentCuffey and Paterson [43]. Firn densification owing to horizontal compression is neglected, although in fast-flowing regions this can be locally important (Horlings et al. [44]).

In the model update, we recalibrated the dry densification correction factor MO as a function of mean annual accumulation, by using an updated, high-resolution GrIS accumulation field (Noël et al. [45]) and optimizing the modelled depths at which the firn density reaches the critical values $550/830\,\mathrm{kg\,m^{-3}}$ (Ligtenberg et al. [35], Kuipers Munneke et al. [4]) (Fig. 3). To perform the previous calibration, Kuipers Munneke et al. [4] used 22 cores, here we use 29 cores. Since MO corrects for the dry compaction rate, only

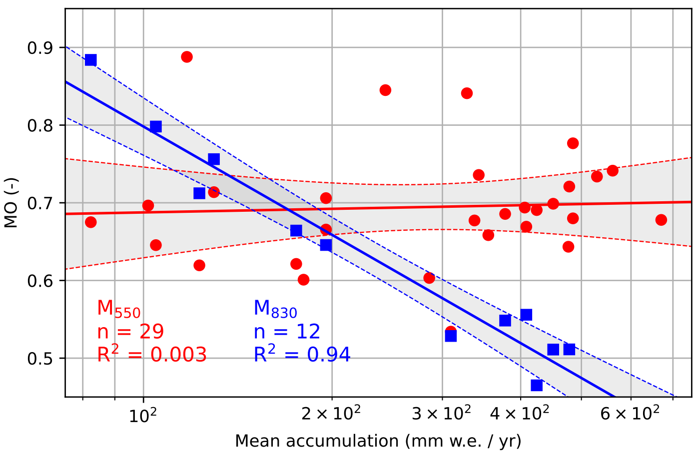

Figure 3: Ratio between modelled and observed depth at which the density reaches $550\,\mathrm{kg\,m^{-3}}$ (MO_{550}) or $830\,\mathrm{kg\,m^{-3}}$ (MO_{830}) as a function of local accumulation rate. The solid lines represent the corresponding regressions and the grey bands around them are their corresponding 95 % confidence intervals.

dry firn cores (i.e. with little surface melt) are used. A core is considered as "dry" if the ratio R_{MA} between the mean annual melt and accumulation is less than 0.05. Least squares fitting yields R^2 for MO_{550} and MO_{830} of $2.82 \cdot 10^{-3}$ and 0.94 respectively. The statistics of the new and old fit are summarised in table 1.

With the update and extension of firn and accumulation data, the linear relation between MO_{550} and $\ln(\dot{b})$ vanishes, and reduces to an almost constant value of 0.7. Despite the difference with previous formulations in IMAU-FDM, this is similar to findings by Robin [46] and Herron and Langway [47], who also found that below $550\,\mathrm{kg\,m^{-3}}$ the densification rate correlates almost linearly with accumulation, and at this correlation became non-linear at higher densities. Similarly, the high correlation for MO_{830} also implies that the relation between densification rate $\frac{\mathrm{d}\rho}{\mathrm{d}t}$ and accumulation is non-linear above $\rho = 550\,\mathrm{kg\,m^{-3}}$.

2.2.3. *Thermal conductivity*

In IMAU-FDM, the vertical temperature distribution and its evolution is obtained by solving the one-dimensional heat transfer equation

$$\rho c \frac{\partial T}{\partial t} = -\frac{\partial G}{\partial z} + \mathcal{L} = -\frac{\partial}{\partial z}\left(k \frac{\partial T}{\partial z}\right) + \mathcal{L} \tag{5}$$

in which c is the specific heat capacity of the firn, G the subsurface heat flux, k the thermal conductivity of the firn and $\mathcal{L}$ a heat source representing the release of latent heat upon the refreezing of liquid water in the firn or the subsurface absorption of solar radiation. Subsurface penetration of shortwave radiation is neglected in the current model version, which is deemed a reasonable approximation for fine-grained, polar snow surfaces. The firn temperature profile is initialized using a spin-up period, see Section 2.2.5. Before the spin-up, the firn column is initialised at a constant temperature equal to the annual mean surface temperature during the spin-up period. The lower boundary condition assumes a constant heat flux across the lowest model grid cell, i.e. the deep temperature is allowed to change along with long-term changes in surface temperature or internal heat release. The upper boundary condition for the temperature calculation is provided by the surface ('skin') temperature in RACMO2, obtained by iteratively solving the surface energy balance (Van Den Broeke et al. [48]). Subsequently, for computational efficiency Eq. 5 is solved using an implicit/explicit scheme in the absence/presence of liquid water (Helsen et al. [49]). Due to the Lagrangian character of the model, vertical heat advection is implicitly consideredHelsen et al. [49]. Any heat generated by firn horizontal/vertical deformation is neglected.

The thermal conductivity is assumed to depend on firn density and temperature, and in previous versions of IMAU-FDM followed the expression for seasonal snow due to Anderson [50], which only depends on density. In the updated model, the parameterization for thermal conductivity as a function of firn density of Calonne et al. [51] replaces the expression of Anderson [50] in order to more accurately model the dynamics of the thermal conductivity by incorporating both a density and temperature dependency. The new expression was obtained from 3D images of firn micro-structures at different

Table 1: Values of the old and new linear regression of Eq. 4, their R^2 as well as the standard error in of the new fitting parameters.

	α_{old}	α_{new}	σ_α	β_{old}	β_{new}	σ_β	R^2_{old}	R^2_{new}
MO_{550}	1.042	0.6569	0.1367	0.0916	-0.0067	0.0242	0.35	0.003
MO_{830}	1.734	1.7243	0.0880	0.2039	0.2011	0.0161	0.96	0.940

temperatures, and is valid for the wide range of density and temperature values typically encountered in ice sheet firn layers, making it suitable for simulations of the GrIS. It takes on the following form:

$$k(\rho, T) = (1 - \theta)\frac{k_i(T)k_a(T)}{k_i(-3\,^\circ\mathrm{C})k_a(-3\,^\circ\mathrm{C})}k_{snow}(\rho) + \theta\frac{k_i(T)}{k_i(-3\,^\circ\mathrm{C})}k_{firn}(\rho) \qquad (6)$$

The equation consists of two parts: one for snow and low-density firn and one for ice and high-density firn. The transition between the two regimes remains smooth through the weight factor $\theta(\rho)$. The definition of θ and the thermal conductivities that are used in Eq. 6 are:

$$\begin{aligned}
\theta &= 1/(1 + \exp(-0.04(\rho - 450)) \\
k_i(T) &= 9.828\exp(-0.0057T) \\
k_a(T) &= (2.334 \cdot 10^{-3}T^{3/2})/(164.54 + T) \\
k_{snow}(\rho) &= 0.024 - 1.23 \cdot 10^{-4}\rho + 2.5 \cdot 10^{-6}\rho^2 \\
k_{firn}(\rho) &= 2.107 + 0.003618(\rho - \rho_i)
\end{aligned}$$

Here k_a represents the thermal conductivity of air, taken from Reid et al. [52]. Figure 4 compares the old and new expressions for various temperatures. As can be seen, the new expression takes on a slightly lower value than Anderson [50] at densities below $\sim 475 - 565$ kg m^{-3}, depending on the temperature, but a higher value at densities above that. This difference becomes larger at lower temperatures.

2.2.4. Meltwater percolation, retention and refreezing

IMAU-FDM employs a tipping bucket method to treat the percolation, irreducible (capillary) retention and (re)freezing of water, by filling up subsequent deeper layers to maximum capacity in a single model time step (i.e. quasi-instantaneous). Magnusson and others (Magnusson et al. [53]) show that, in spite of its simplicity and shortcomings, the tipping bucket method is a robust and useful method to deal with liquid water transport in the snowpack when compared to more sophisticated methods, especially when capturing general firn properties at the larger, multi-kilometre horizontal scale for which IMAU-FDM is designed. In IMAU-FDM, the fraction that is

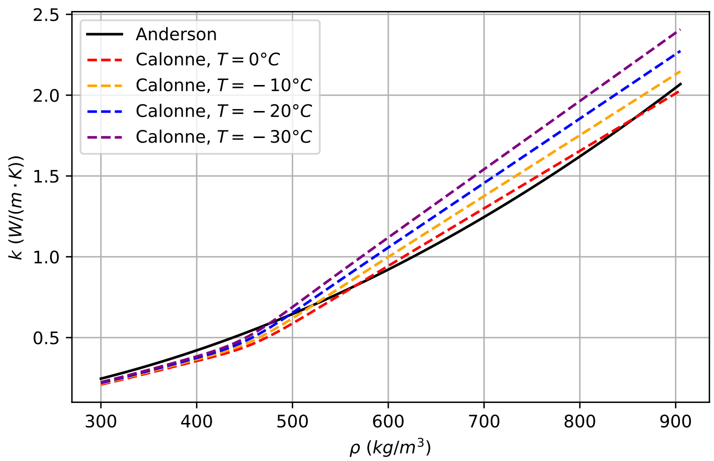

Figure 4: Comparison of the thermal conductivity parameterisation by Anderson [50] and Calonne et al. [51] with density at different temperatures.

retained in a model layer by capillary forces ('irreducible water content') depends on the available pore space according to the expression due to Colèou and LessafreColéou and Lesaffre [54]:

$$W_c = 1.7 + 5.7\frac{P}{1-P} \tag{7}$$

where P is the porosity of the firn layer, defined as $P = 1 - \rho/\rho_i$. The maximum amount of water that is stored thus decreases with increasing density of the firn layer. Standing water and lateral runoff over ice-layers are currently ignored; the latter is considered a fair assumption, because on the spatial scales at which the model is employed (i.e. the RACMO2 grid of 5.5 by 5.5 km^2) it is assumed that within a model grid cell the meltwater can usually find a way to flow around a layer of ice. Varying the irreducible water content by, e.g., multiplying Eq. 7 with a constant factor or using a constant volume or mass fraction, did not improve the result, and it was decided to leave the liquid water scheme unchanged.

2.2.5. Model initialisation

The latest IMAU-FDM model runs span the period 1 January 1960 - 31 December 2020. The initial model density, temperature and liquid water content in the firn column are obtained by repeatedly applying the spin-up period 1960 - 1979 during which the forcing (i.e. surface accumulation, liquid water flux and temperature) is assumed to have remained reasonably constant (i.e. no significant trends, Van Den Broeke et al. [55]). Observations and model studies support the assumption that the Greenland climate and SMB started to change significantly in the 1990sEnderlin et al. [56], McMillan et al. [57], confirming that the period 1960 - 1979 can be selected for initialization purposes. Initialization is considered complete when the entire firn layer (up to the pore close-off density of $830\,\mathrm{kg\,m^{-3}}$) has been refreshed. The required number of iterations depends on accumulation rate, and is typically 10 to 20 for the relatively dry grid points in the northeastern GrIS and typically 25 to 45 for the relatively wet southeastern GrIS. After the spin-up is finished, the model completes the run by once applying the 1980-2020 forcing from RACMO2.3p2.

2.3. RACMO2.3p2 forcing

At the upper boundary of IMAU-FDM, mass accumulation (solid precipitation minus sublimation minus drifting snow erosion), liquid water fluxes (melt plus rainfall minus evaporation) and surface temperature are prescribed from the regional atmospheric climate model RACMO2.3p2, which has been used to simulate the climate and surface mass balance of the GrIS and its immediate surroundings for the period 1958-2020 at a horizontal resolution of 5.5 km. This version of RACMO2 has been extensively evaluated over the Greenland ice sheet (Noël et al. [20]). At the lateral boundaries, using a relaxation zone of 24 gridpoints, RACMO2 is forced by European Centre for Medium-Range Weather Forecasts (ECMWF) re-analysis data, i.e. ERA-40 between 1958 and 1978, ERA-Interim between 1979 and 1990 and ERA-5 between 1991 and 2020. For the forcing of IMAU-FDM the full spatial resolution of 5.5 km is used and a temporal resolution of 3 hours was selected, as an acceptable trade-off between robustly resolving the daily cycle and keeping manageable file sizes. IMAU-FDM typically uses a timestep of 3 min (explicit temperature calculation scheme) to 3 h (implicit temperature calculation scheme), for which we linearly interpolate the forcing between the RACMO2 forcing time steps.

3. Model performance

3.1. Firn density

The vertical density profiles of 92 GrIS firn cores are used to assess the performance of the updated model. For each available firn core, IMAU-FDM

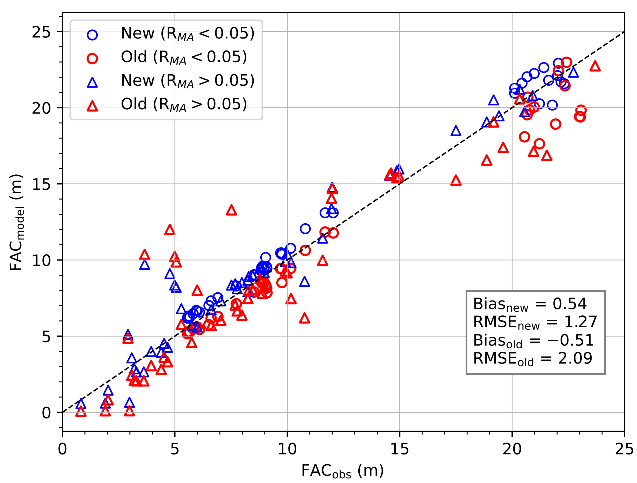

Figure 5: Modelled vs observed firn air content in metres. Dry locations are indicated with circles whereas wet locations are indicated with triangles.

has been run at the grid point closest to that location. The evaluation is not completely independent of the calibration, as the cores used for fitting the MO-values are also included. As an integrated measure of porosity, we compare modelled and observed vertically integrated firn air content (FAC), i.e. the vertical distance over which the firn layer can be compressed until reaching the density of glacier ice everywhere.

$$\mathrm{FAC} = \sum_{j}^{n_z} \frac{(\rho_i - \rho_j)}{\rho_i} \Delta z_j \tag{8}$$

Here, n_z is the number of layers in that firn profile, Δz_j is the thickness of layer j and ρ_j is the density of that layer. Note that here the FAC is calculated over the complete depth at which observations are available, as opposed to FAC_{10} shown in Fig. 1 which was calculated over the top 10 m. FAC is an indicator of the meltwater retention capacity of the firn layer and therewith an important parameter to simulate correctly. In general, one can state that locations on the GrIS with FAC > 15 m (Fig. 1) experience little to no melt, whereas the locations with FAC < 15 m do experience significant melt and refreezing, which uses up part of the pore space.

With the newly adopted parametrizations, the simulation of FAC in dry locations has significantly improved (Fig. 5). For these 39 locations, the mean bias and root mean squared error (RMSE) decreased from $-0.98/1.45$ to $0.56/0.83$ metre, respectively. The improvement is more modest for low FAC locations, where the previous underestimation has been replaced with a small overestimation. For these 53 locations, the mean bias / RMSE changed from $0.02/2.53$ to $0.65/1.58$ metre, respectively. For all cores combined, the mean bias and RMSE have decreased from $-0.40/2.14$ to $0.61/1.32$ metre respectively.

[40] noted that surface density correlates only weakly with annual mean T_a and that using a constant density of $315\,\mathrm{kg\,m^{-3}}$ may be preferable. To assess this, we compared FAC for the old model and the new model with and without temperature dependence. In order to identify possible depth-dependent biases we also define a cost function, Φ, to quantify the error in the modelled density profile:

$$\Phi = \sqrt{\frac{1}{n_z}\sum_{i}^{n_z}\left(\rho_{model,i} - \rho_{obs,i}\right)^2} \tag{9}$$

The RMSE in FAC decreased from $2.14\,\mathrm{m}$ with the old settings, to $1.32\,\mathrm{m}$ with the new settings, including a temperature dependent surface snow density and $1.44\,\mathrm{m}$ when using a constant surface snow density of $315\,\mathrm{kg\,m^{-3}}$. Similarly, the mean Φ of all density profiles decreased from $50.3\,\mathrm{kg\,m^{-3}}$ to 44.4 and $41.0\,\mathrm{kg\,m^{-3}}$ respectively when using the new settings with and without temperature dependency for surface snow density. These results show that including temperature as a predictor for the surface density does improve model performance, but only marginally so. Nevertheless, we opt for the temperature dependent formulation since this allows capturing the effect of long-term temperature trends on the surface density.

Fig. 6 shows two observed and modelled density profiles from the locations Das2 and FA-13, sites with large and small FAC respectively. Das2 is a dry location, with very little melt and changes to its profile whereas FA-13 experiences a lot of melt. At both sites, the new model settings result lead to an improved overall representation of density-depth profile, with a more realistic shape and reduced variability. It increases the pore space and thus brings simulated FAC in better agreement with the observed density profile. One of the main reason for the increased performance is the change from an instantaneous surface density parameterization to one that is based on annual mean values. This leads to greatly reduced "peaks" in the density

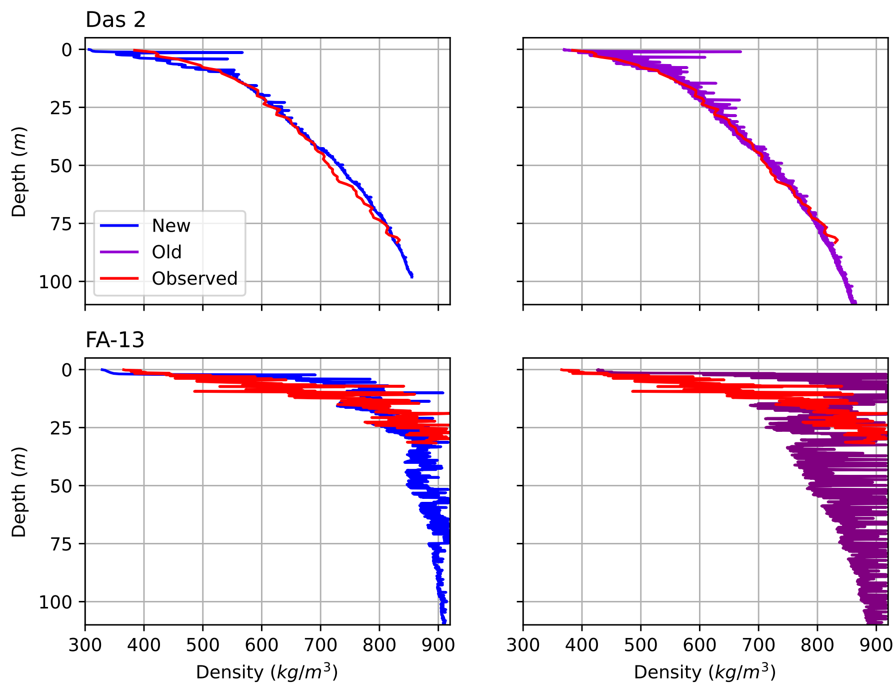

Figure 6: Density profiles for the new (left) and old (right) model settings at Das 2 (top) and FA-13 (bottom).

profile, which is much more in line with observations since the surface density. For FA-13, it also seems that the lower surface density matches the upper ~ 25 m of the density profile better.

3.2. Firn temperature

Modelled and measured 10 m firn temperatures at 31 locations are compared in Fig. 7. The new settings improve results, especially for the warmer locations with significant melt, which are mostly locations from Harper-Harper et al. [58] in west Greenland. Here, the cold bias has been significantly reduced; for locations with $T_{10} > -20\,°\mathrm{C}$, the mean bias/RMSE decreased from $-2.5/4.7$ to $-0.8/2.7$ °C, respectively.

The main reason for this is a better representation of the density at those locations, which allows for improved representation of refreezing and the associated enhanced latent heat release, increasing the temperature in

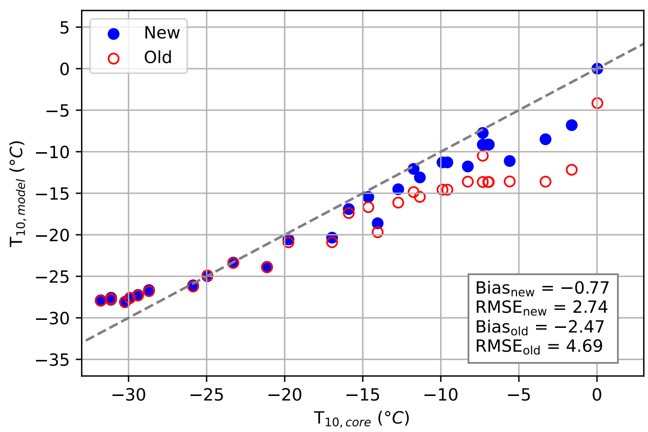

Figure 7: Modelled vs. observed temperature at 10 m depth (in °C) for 31 locations on the GrIS.

these melt-prone locations. In spite of the clear improvement, a cold-bias remains for some of these locations, which could also be partly attributed to a cold-bias in the RACMO2 forcing.

For the low-melt locations ($T_{10} < -20\,$°C), a persistent warm model bias remains. Because RACMO2.3p2 is known to accurately simulate near-surface air temperature over the GrIS (Noël et al. [20]).

Fig. '8 compares the observed temperature profiles of Summit and Dye-2 in the winter and the summer with the new and old model results. Similarly to what was found in Fig. 7, Summit, which is a dry and cold location contains a warm bias whereas Dye-2, which is warm and wet, contains a cold bias. For both locations the new surface density parameterization has decreased its density in the upper layers. This in turn also leads to a lower thermal conductivity since the thermal conductivity increases monotonically with density (see Fig. 4). Therefore, most of the heat or cold stays in the upper layers and the temperature gradient is larger there, which can be seen clearly at Summit. For both locations the depth at which the thermal maximum occurs also increased slightly.

Lastly, Dye-2 now clearly shows a maximum in the temperature at the depth at which refreezing occurs which does not occur with the old model settings. This is also attributed to a decrease in the thermal conductivity: previously, heat generated by refreezing was able to escape to greater depths

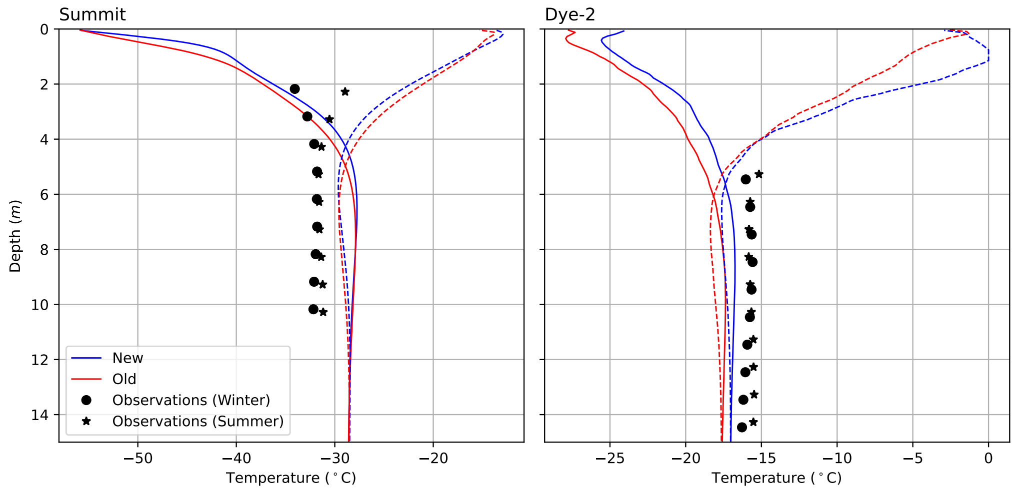

Figure 8: Comparison between observed temperature profiles vs. the new settings and the old model results in summer (dashed lines) and winter (solid lines) at Summit in winter (9 March 2002) and summer (6 August 2002) and Dye-2 in the summer (10 August 2007) and winter (13 March 2007).

or the atmosphere, but now it remains "trapped" around the depth at which refreezing occurs. Another factor that contributes to this is that refreezing occurs at a greater depth than before, see section 3.3.

3.3. Liquid water content

The liquid water percolation and retention schemes have not been updated, but the changes made to the parameterizations that impact density and temperature do influence water percolation, and therewith liquid water content (LWC), and these changes are discussed here. Very few in-situ, vertically resolved observations of LWC are available. A recent study used upward looking ground penetrating radar (upGPR) at Dye-2 in the higher percolation zone of the southwestern GrIS (2120 m a.s.l., see Fig. 1, Heilig et al. [59]). Even though the data do not cover a wide spatial (single location) or temporal range (1 May - 16 October 2016), they are unique and moreover have high temporal and vertical resolution, making them very valuable for firn model evaluation (Vandecrux et al. [19]), but also e.g. to evaluate melt intensity and timing in the forcing time series.

Fig. 9 compares both the old and the new model results against the observed evolution of the maximum penetration depth and LWC in the firn.

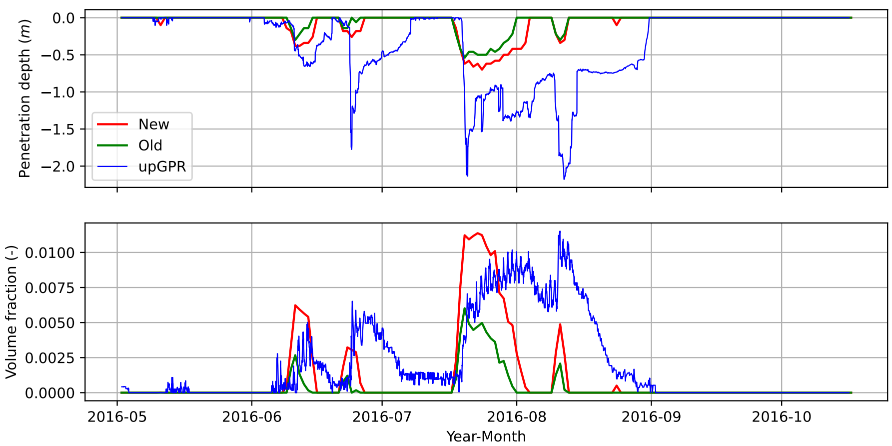

Figure 9: Comparison between the observed penetration depth (top) and volume fraction (bottom) of liquid water at Dye-2 with the new and old model results.

The measurements reveal that the melt in 2016 at Dye-2 mostly occurred in four periods between July and October, the timings of which are well captured in the RACMO2.3p2 forcing. Comparing old and new model settings, the water penetration depth and LWC have both increased. This mainly reflects the decreased density in the upper layer at Dye-2. As discussed in the previous section, this leads to an increase in the temperature in the upper firn layer and stronger gradients at Dye-2. The increase in temperature means that the water needs to percolate deeper into the firn pack before it can refreeze, which is reflected in the increased penetration depth. Simultaneously, the decrease of the surface density means that there is more pore space near the surface that can retain water as irreducable water content, explaining the increase in volume fraction. Overall, the penetration depth now agrees better with the observations, although the meltwater still refreezes too quickly in IMAU-FDM compared to the observations.

4. Pilot application to firn-induced surface elevation change

In this section we compare time series (1958-2020) of firn-induced surface elevation (i.e. firn depth) changes at three key locations: Summit in the cold and dry ice sheet interior, KAN-U in the relatively warm and dry southwestern percolation zone and FA-13 in the wet and relatively mild southeastern firn aquifer region (Koenig et al. [32], Forster et al. [60], as indicated by the green circles in Fig. 1). Table 2 contains some more information about these locations The three locations represent three very different climates and are therefore useful for investigating how the new model settings affect the evolution of the height of the firn column in these different circumstances. Here we focus on the cumulative firn depth change at the three sites, which represent the predicted elevation change in the abscence of contributions from ice dynamics, basal melt and/or bedrock elevation change. The three sites show very different responses to contemporary decadal and interannual Greenland climate variability, as will be discussed below.

4.1. Summit

Summit is an interesting location because it is located at the centre of the GrIS at a high elevation and therefore it experiences a low amount of snowfall and little to no rain and melt. The evolution of its elevation is therefore closely linked to changes in the temperature (higher temperatures lead to a higher compaction rate) and accumulation (higher accumulation leads to a higher surface elevation). The model is at the surface forced by the skin temperature and the accumulation. Fig. 10 shows how the mean annual accumulation and mean annual skin temperature change over the course of the simulation period, as well as changes to the surface elevation and its velocity components for the new and old settings.

At Summit, 1.5 m elevation change between 1975 and 2005 ($\sim 5\,\mathrm{cm\,yr^{-1}}$) is modelled, with relatively stable firn depth in the periods before and after. If we look at the associated climate forcing, this can be explained by a small decrease in accumulation since about 2000, along with slightly increased temperatures since that period. Differences between old and new model settings are small, despite the individual velocity components being very different.

Table 2: Location and climate climate of the three case study sites. The annual mean accumulation are calculated over the whole simulation period (1957-2020).

	Lon. (°W)	**Lat.** (°N)	**Elevation** (m a.s.l.)	$T_{2\,\mathrm{m}}$ (°C)	**Acc.** (mm w.e.)	**Melt** (mm w.e.)
Summit	-38.32	72.55	3281	-26.0	206	0
KAN-U	-47.02	67.00	1840	-12.4	480	271
FA-13	-39.04	66.18	1563	-7.0	986	496

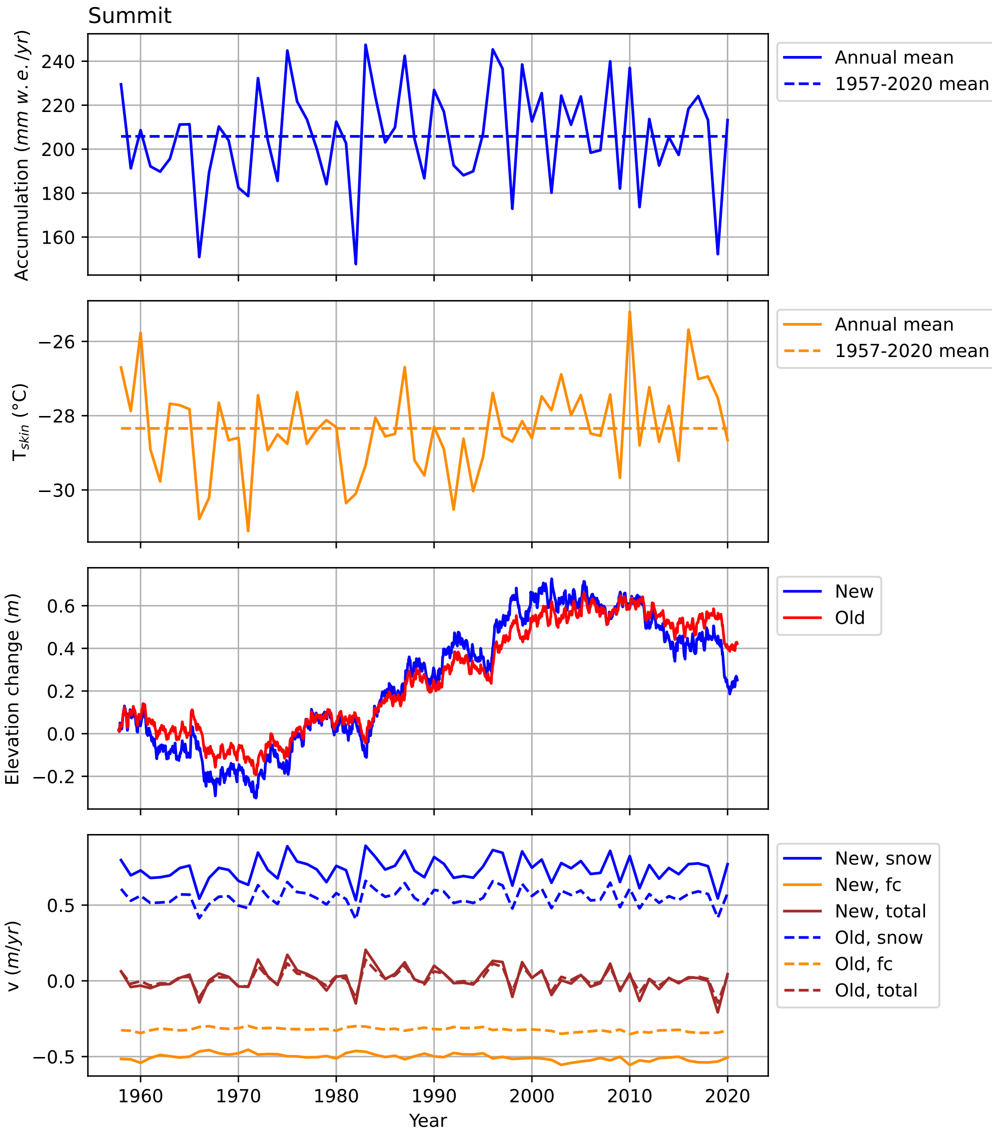

Figure 10: Time series of the total annual accumulation , the annual mean skin temperature, the height change and mean annual velocity components at Summit.

The firn model can be conveniently used to quantify the relative contributions of the various components of firn depth changes, expressed as a vertical velocity: snowfall (v_{snow}), sublimation (v_{sub}), drifting snow erosion (v_{snd}), melt (v_{melt}) and firn compaction (v_{fc}). At Summit, interannual variability in firn depth is dominated by snowfall (v_{snow}), which is compensated mainly by steady firn compaction (v_{fc}), which are shown in the bottom graph in Fig. 10. From this it follows that the slightly higher accumulation and lower temperature between 1975 and 2005 caused the upward surface velocity due to accumulation to decrease, and the downward velocity due to compaction to increase. As a result, net vertical velocity reduces to almost zero, leading to a relatively stable surface elevation. Overall, the net vertical velocity of the surface is very similar between the old and the new version. However, when looking at its velocity components we notice that both v_{snow} and v_{fc} have increased in size equally. The new surface density parameterization (Eq. 1) leads to a lower surface density, which in turn increases the rate at which the surface elevation increases since the height deposited during a snow event is equal to m/ρ_{snow}, with m being the mass being deposited. This is then compensated for by larger MO values during (MO_{550} has increased from 0.56 to 0.69 and MO_{830} has increased from 0.62 to 0.66 respectively). This explains why overall v_{total} does not differ much between the old and new settings.

However, the new settings do result in larger seasonal and interseasonal swings in the firn depth. This is because v_{snow} and v_{fc} act on different timescales. v_{fc} is fairly constant in time and changes in tandem with the seasonal changes in temperature. v_{snow} on the other hand occurs much more sporadically. As a result, the surface elevation increases more during a snowfall event and decreases faster when there is no such event, leading to larger interannual variations. This also implies that the firn model has become more sensitive to changes in the forcing, reacting more strongly to a decrease or increase in the accumulation or skin temperature in the future.

4.2. KAN-U

KAN-U is a very different location than Summit. Situated in the southwest and at a higher elevation it is warmer but most importantly melting occurs every year during the summer, which greatly affects the firn properties at its location. The average influence of surface melt on firn depth changes (v_{melt}) is similar to the contribution made by compaction (v_{fc}): it decreases the depth of the firn column and decreases its air content. Fig. 11 shows the time series at KAN-U.

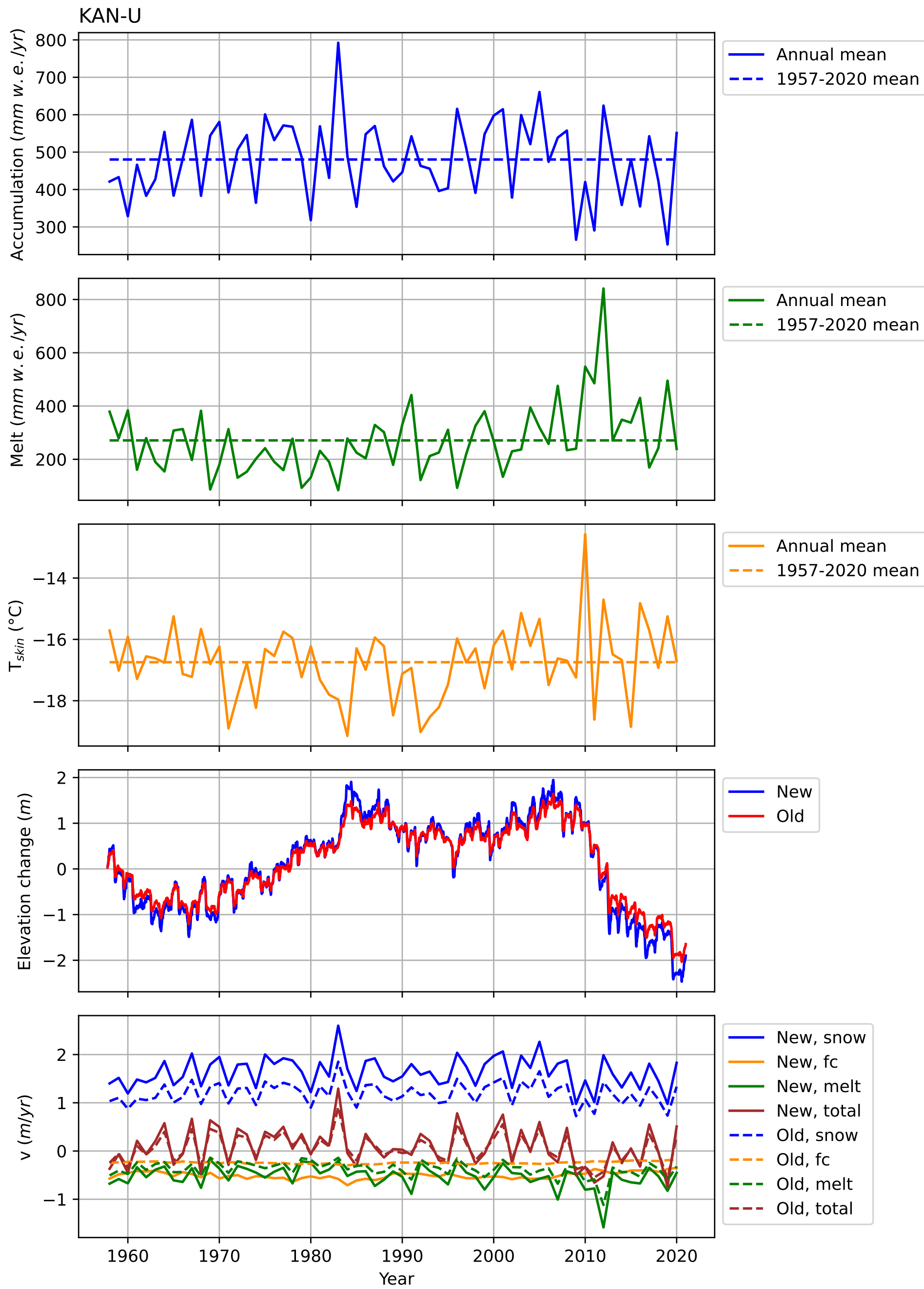

Figure 11: Time series of annual accumulation, melt, annual mean skin temperature, surface elevation change and mean annual vertical velocity components at KAN-U.

At KAN-U, a 2.5 m thickening is modelled between 1970 and 1985. If we look at the associated climate forcing, this can be explained by a relatively low amount of melt and temperature during this period. Between 2005 and 2020 ($-20\,\mathrm{cm\,yr^{-1}}$) an even rapid decline of even greater magnitude ($-20\,\mathrm{cm\,yr^{-1}}$) is observed, which may be associated with a strong increase in surface melt since 2005, as well as a slight increase in temperature and a reduction in the number of high-accumulation years. KAN-U experienced a very cold and wet year in 1983 as well as a very warm year in 2010 and a lot of melt in 2012 which greatly affect its elevation, which otherwise changes relatively gradual.

In terms of vertical surface velocities, the new model settings cause the accumulation velocity to increase, due to a lower fresh snow density. This is again compensated for by a more negative compaction velocity, resulting in a very similar net velovity (v_{tot}). As accumulation reduces after 2005, the net effect on the surface is a slight lowering. Following significant warming and increased melt at this site (Fig. 11), the contribution of v_{melt} to firn depth changes increases and that of v_{fc} decreases, making the former the dominant process leading to surface lowering at KAN-U. The strong increase in melt causes a larger downward velocity of the surface, leading to thinning. v_{melt} is also larger in magnitude with the new settings than with the old settings because the melted snow at the surface is at a lower density.

Just like at Summit, the elevation change seems to be more sensitive to its forcing with the new model settings than previously was the case. This is especially apparent in the years 1983 and 2012. In the beginning of the time series, interannual variability in firn depth is dominated by snowfall (v_{snow}), but towards the end of the time series the contribution to the total variability made by v_{melt} increases rapidly.

4.3. FA-13

While at the two previous sites the new model settings produce similar results for the long-term trends, a significant difference is found at FA-13. This location experiences an even warmer and wetter climate than KAN-U which lead to a rapid densification as has been shown in Fig. 6.

Here, the signal is dominated by large oscillations in firn depth up to $\sim 1\,\mathrm{m\,yr^{-1}}$ between 1960 and 1985. From 1985 onwards, the firn depth decreases until 2012, but at a higher rate in the updated than in the previous model (~ 0.35 vs. $0.25\,\mathrm{m\,yr^{-1}}$). This is where the new settings show a

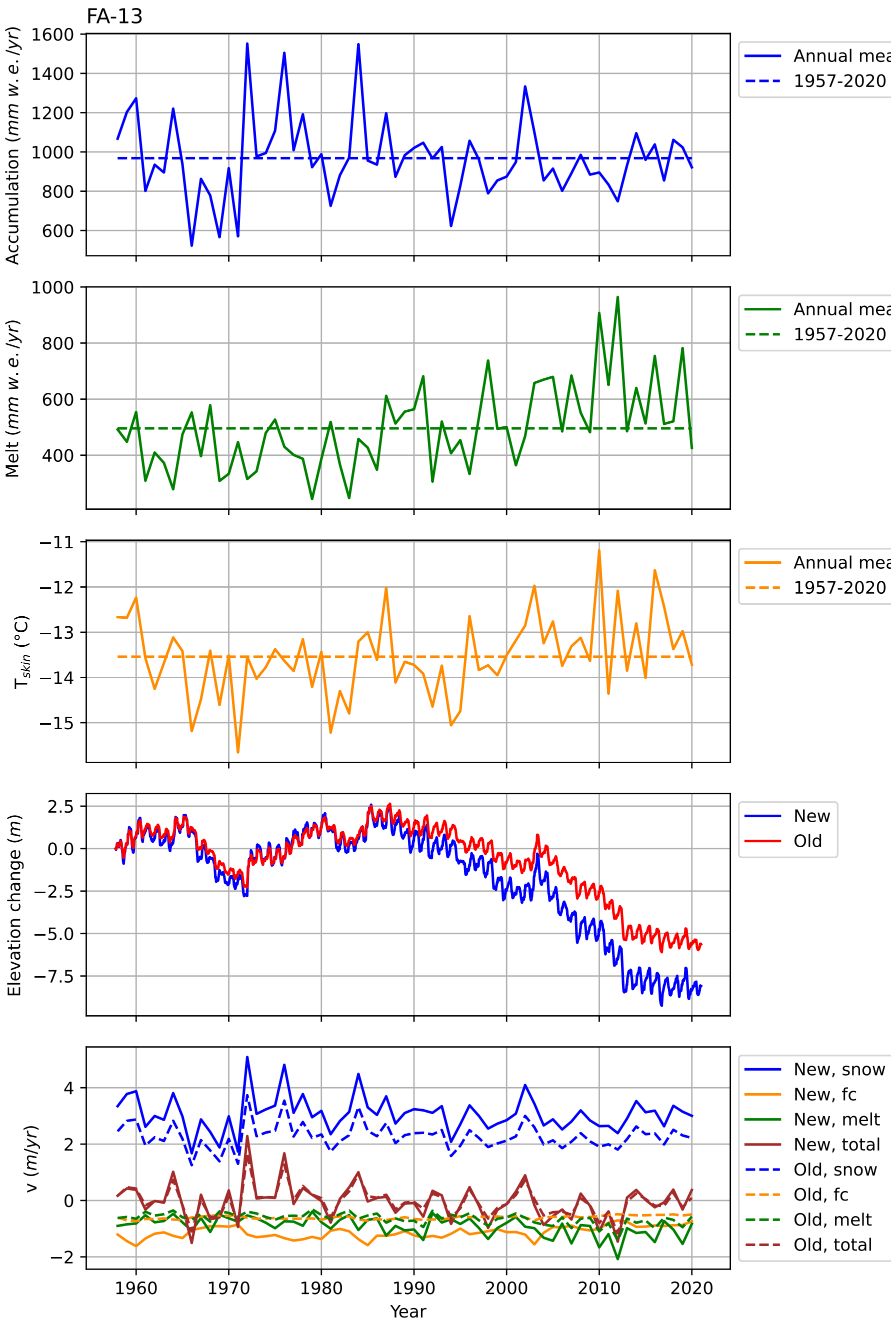

Figure 12: Time series of annual accumulation, melt, annual mean skin temperature, surface elevation change and mean annual vertical velocity components at FA-13.

For its velocity components, a similar picture emerges at FA-13 as at KAN-U, where a significant melt increase means that v_{melt} becomes the dominant source of annual firn thinning since 2005. v_{melt} also increases its relative contribution to interannual firn thickness variability, partly because variability in v_{snow} is decreasing. The new model settings at FA-13 show the same signature in the individual vertical-velocity components as at the other two sites: accumulation leads to more surface thickening due to the lower fresh-snow density. To compensate, compaction also increases. The compaction in the new model set-up is stronger and shows more interannual variability, in line with the larger interannual variability of the annual accumulation height.

Vertical surface velocity due to surface melt is very different in the new model version compared to the old one. Both the variability and the magnitude of the melt is stronger in the new model. At site FA-13, melt is a significant fraction of the annual accumulation. In the period 1990-2020, 8.5 m of thinning occurred in the new model, compared to 6 m in the old model. Since the uppermost layers of snow are structurally less dense in the new model, surface melt implies a stronger lowering of the surface for less dense snow, as demonstrated in Fig 11 and 12. It is clear that the new model has larger downward surface velocity than the old model especially in strong melt years. It corroborates the idea that strong melt events over less dense snow lead to stronger surface lowering.

5. Summary and outlook

Temporal and spatial variability in firn thickness is highly relevant for the mass balance of the Greenland ice sheet (GrIS), because it directly impacts its refreezing efficiency. Moreover, firn thickness change is an important component of surface elevation change, and improved knowledge is required to accurately convert remotely sensed GrIS volume to mass changes. Here we present improvements in the offline version of the firn densification model IMAU-FDM, forced by three-hourly output of the regional climate model RACMO2.3p2. Taking advantage of improved climate forcing and newly available observations of surface and subsurface firn density and temperature, the improvements are systematically implemented in the parametrizations of surface density, dry snow densification and thermal conductivity. The treatment of liquid water is not changed, owing to a lack of sufficient observations to justify changes in the current configuration.

The updated model predicts generally higher firn air content (FAC), which at three selected sites in the interior GrIS and in the southwestern and southeastern percolation zone results in a larger sensitivity of firn thickness to intra- and interannual variations in snowfall, melt and temperature. As an important consequence of a change in fresh snow density parameterization, the inter- and intra-annual variations in elevation have increased, owing to an increased sensitivity to changes in its forcing. In a warmer climate, firn thinning owing to increased surface melt becomes increasingly important at the marginal sites, both in the mean and as a component of interannual variability. Future applications of the improved model include a full GrIS assessment of contemporary and future firn mass and thickness changes, as well as explaining areas where firn aquifers and ice slabs currently occur, and their future changes.

References

[1] B. Noël, W. J. van de Berg, S. Lhermitte, B. Wouters, N. Schaffer, M. R. van den Broeke, Six Decades of Glacial Mass Loss in the Canadian Arctic Archipelago, Journal of Geophysical Research: Earth Surface 123 (2018) 1430–1449.

[2] B. Noël, W. J. van de Berg, S. Lhermitte, B. Wouters, H. Machguth, I. Howat, M. Citterio, G. Moholdt, J. T. M. Lenaerts, M. R. van den Broeke, A tipping point in refreezing accelerates mass loss of Greenland's glaciers and ice caps, Nature Communications 8 (2017) 14730.

[3] B. Noël, C. L. Jakobs, W. J. van Pelt, S. Lhermitte, B. Wouters, J. Kohler, J. O. Hagen, B. Luks, C. H. Reijmer, W. J. van de Berg, M. R. van den Broeke, Low elevation of Svalbard glaciers drives high mass loss variability, Nature Communications 11 (2020) 1–8.

[4] P. Kuipers Munneke, S. R. Ligtenberg, B. P. Noël, I. M. Howat, J. E. Box, E. Mosley-Thompson, J. R. McConnell, K. Steffen, J. T. Harper, S. B. Das, M. R. Van Den Broeke, Elevation change of the Greenland Ice Sheet due to surface mass balance and firn processes, 1960-2014, Cryosphere 9 (2015) 2009–2025.

[5] B. Vandecrux, M. MacFerrin, H. MacHguth, W. T. Colgan, D. Van As, A. Heilig, C. Max Stevens, C. Charalampidis, R. S. Fausto, E. M.

Morris, E. Mosley-Thompson, L. Koenig, L. N. Montgomery, C. Miège, S. B. Simonsen, T. Ingeman-Nielsen, J. E. Box, Firn data compilation reveals widespread decrease of firn air content in western Greenland, Cryosphere 13 (2019) 845–859.

[6] M. R. Van Den Broeke, E. M. Enderlin, I. M. Howat, P. Kuipers Munneke, B. P. Noël, W. Jan Van De Berg, E. Van Meijgaard, B. Wouters, On the recent contribution of the Greenland ice sheet to sea level change, Cryosphere 10 (2016) 1933–1946.

[7] J. Harper, N. Humphrey, W. T. Pfeffer, J. Brown, X. Fettweis, Greenland ice-sheet contribution to sea-level rise buffered by meltwater storage in firn, Nature 491 (2012) 240–243.

[8] J. Mouginot, E. Rignot, A. A. Bjørk, M. van den Broeke, R. Millan, M. Morlighem, B. Noël, B. Scheuchl, M. Wood, Forty-six years of Greenland Ice Sheet mass balance from 1972 to 2018, Proceedings of the National Academy of Sciences of the United States of America 116 (2019) 9239–9244.

[9] S. V. Nghiem, D. K. Hall, T. L. Mote, M. Tedesco, M. R. Albert, K. Keegan, C. A. Shuman, N. E. DiGirolamo, G. Neumann, The extreme melt across the Greenland ice sheet in 2012, Geophysical Research Letters 39 (2012) 6–11.

[10] I. Sasgen, B. Wouters, A. S. Gardner, M. D. King, M. Tedesco, F. W. Landerer, C. Dahle, H. Save, X. Fettweis, Return to rapid ice loss in Greenland and record loss in 2019 detected by the GRACE-FO satellites, Communications Earth & Environment 1 (2020).

[11] C. R. Steger, C. H. Reijmer, M. R. Van Den Broeke, The modelled liquid water balance of the Greenland Ice Sheet, Cryosphere 11 (2017) 2507–2526.

[12] H. Machguth, M. MacFerrin, D. Van As, J. E. Box, C. Charalampidis, W. Colgan, R. S. Fausto, H. A. J. Meijer, E. Mosley-Thompson, R. S. W. van de Wal, Greenland meltwater storage in firn limited by near-surface ice formation, Nature Climate Change 6 (2016) 390–393.

[13] M. MacFerrin, H. Machguth, D. van As, C. Charalampidis, C. M. Stevens, A. Heilig, B. Vandecrux, P. L. Langen, R. Mottram, X. Fettweis, M. R. den Broeke, W. T. Pfeffer, M. S. Moussavi, W. Abdalati, Rapid expansion of Greenland's low-permeability ice slabs, Nature 573 (2019) 403–407.

[14] H. J. Zwally, J. Li, J. W. Robbins, J. L. Saba, D. Yi, A. C. Brenner, Mass gains of the Antarctic ice sheet exceed losses, Journal of Glaciology 61 (2015) 1019–1036.

[15] B. Wouters, A. Martin-Español, V. Helm, T. Flament, J. M. Van Wessem, S. R. Ligtenberg, M. R. Van Den Broeke, J. L. Bamber, Dynamic thinning of glaciers on the Southern Antarctic Peninsula, Science 348 (2015) 899–903.

[16] A. Shepherd, E. Ivins, E. Rignot, B. Smith, M. van den Broeke, I. Velicogna, P. Whitehouse, K. Briggs, I. Joughin, G. Krinner, S. Nowicki, T. Payne, T. Scambos, N. Schlegel, G. A, C. Agosta, A. Ahlstrøm, G. Babonis, V. R. Barletta, A. A. Bjørk, A. Blazquez, J. Bonin, W. Colgan, B. Csatho, R. Cullather, M. E. Engdahl, D. Felikson, X. Fettweis, R. Forsberg, A. E. Hogg, H. Gallee, A. Gardner, L. Gilbert, N. Gourmelen, A. Groh, B. Gunter, E. Hanna, C. Harig, V. Helm, A. Horvath, M. Horwath, S. Khan, K. K. Kjeldsen, H. Konrad, P. L. Langen, B. Lecavalier, B. Loomis, S. Luthcke, M. McMillan, D. Melini, S. Mernild, Y. Mohajerani, P. Moore, R. Mottram, J. Mouginot, G. Moyano, A. Muir, T. Nagler, G. Nield, J. Nilsson, B. Noël, I. Otosaka, M. E. Pattle, W. R. Peltier, N. Pie, R. Rietbroek, H. Rott, L. Sandberg Sørensen, I. Sasgen, H. Save, B. Scheuchl, E. Schrama, L. Schröder, K. W. Seo, S. B. Simonsen, T. Slater, G. Spada, T. Sutterley, M. Talpe, L. Tarasov, W. J. van de Berg, W. van der Wal, M. van Wessem, B. D. Vishwakarma, D. Wiese, D. Wilton, T. Wagner, B. Wouters, J. Wuite, Mass balance of the Greenland Ice Sheet from 1992 to 2018, Nature 579 (2020) 233–239.

[17] J. M. Lundin, C. M. Stevens, R. Arthern, C. Buizert, A. Orsi, S. R. Ligtenberg, S. B. Simonsen, E. Cummings, R. Essery, W. Leahy, P. Harris, M. M. Helsen, E. D. Waddington, Firn Model Intercomparison Experiment (FirnMICE), Journal of Glaciology 63 (2017) 401–422.

[18] C. M. Stevens, V. Verjans, J. Lundin, E. Kahle, A. Horlings, B. Horlings, E. Waddington, The Community Firn Model (CFM) v1.0, Geoscientific Model Development Discussions (2020) 1–37.

[19] B. Vandecrux, R. Mottram, P. L. Langen, R. S. Fausto, M. Olesen, M. Stevens, V. Verjans, A. Leeson, S. Ligtenberg, P. K. Munneke, S. Marchenko, W. V. Pelt, C. Meyer, I. Hewitt, S. B. Simonsen, S. Samimi, H. Machguth, M. Macferrin, M. Niwano, The firn meltwater Retention Model Intercomparison Project (RetMIP): Evaluation of nine firn models at four weather station sites on the Greenland ice sheet (2020).

[20] B. Noël, W. J. van de Berg, J. M. van Wessem, E. van Meijgaard, D. van As, J. T. M. Lenaerts, S. Lhermitte, P. Kuipers Munneke, C. J. P. P. Smeets, L. H. van Ulft, R. S. W. van de Wal, M. R. van den Broeke, Modelling the climate and surface mass balance of polar ice sheets using RACMO2 – Part 1: Greenland (1958–2016), The Cryosphere 12 (2018) 811–831.

[21] S. R. Ligtenberg, P. K. Munneke, B. P. Noël, M. R. Van Den Broeke, Brief communication: Improved simulation of the present-day Greenland firn layer (1960-2016), Cryosphere 12 (2018) 1643–1649.

[22] J. R. McConnell, E. Mosley-Thompson, D. H. Bromwich, R. C. Bales, J. D. Kyne, Interannual variations of snow accumulation on the Greenland Ice Sheet (1985-1996): New observations versus model predictions, Journal of Geophysical Research Atmospheres 105 (2000) 4039–4046.

[23] E. Mosley-Thompson, J. R. McConnell, R. C. Bales, Z. Li, P. N. Lin, K. Steffen, L. G. Thompson, R. Edwards, D. Bathke, Local to regional-scale variability of annual net accumulation on the Greenland ice sheet from PARCA cores, Journal of Geophysical Research Atmospheres 106 (2001) 33839–33851.

[24] E. Hanna, J. McConnell, S. Das, J. Cappelen, A. Stephens, Observed and modeled Greenland Ice Sheet snow accumulation, 1958-2003, and links with regional climate forcing, Journal of Climate 19 (2006) 344–358.

[25] J. R. Banta, J. R. McConnell, Annual accumulation over recent centuries at four sites in central Greenland, Journal of Geophysical Research Atmospheres 112 (2007) 1–9.

[26] J. E. Box, N. Cressie, D. H. Bromwich, J. H. Jung, M. Van Den Broeke, J. H. Van Angelen, R. R. Forster, C. Miège, E. Mosley-Thompson, B. Vinther, J. R. Mcconnell, Greenland ice sheet mass balance reconstruction. Part I: Net snow accumulation (1600-2009), Journal of Climate 26 (2013) 3919–3934.

[27] L. Koenig, J. Box, N. Kurtz, Improving surface mass balance over ice sheets and snow depth on sea ice, Eos 94 (2013) 100.

[28] L. Koenig, L. Montgomery, Surface mass balance and snow depth on sea ice working group (SUMup) snow density subdataset, Greenland and Antarctica, 1950-2018, 2019. URL: `https://arcticdata.io/metacat/metacat?action=read&qformat=default&sessionid=&d` doi:10.18739/A26D5PB2S.

[29] A. J. Orsi, K. Kawamura, V. Masson-Delmotte, X. Fettweis, J. E. Box, D. Dahl-Jensen, G. D. Clow, A. Landais, J. P. Severinghaus, The recent warming trend in North Greenland, Geophysical Research Letters 44 (2017) 6235–6243.

[30] B. Vandecrux, R. Fausto, D. Van As, W. Colgan, P. Langen, K. Sampson, K. Steffen, K. Haubner, T. Ingemann-Nielsen, M. Niwano, J. Box, Heat budget of Greenland firn: observed and simulated changes from 1998-2015, Technical Report, 2019.

[31] C. Charalampidis, D. Van As, J. E. Box, M. R. Van Den Broeke, W. T. Colgan, S. H. Doyle, A. L. Hubbard, M. MacFerrin, H. Machguth, C. J. P. Smeets, Changing surface-atmosphere energy exchange and refreezing capacity of the lower accumulation area, West Greenland, Cryosphere 9 (2015) 2163–2181.

[32] L. S. Koenig, C. Miège, R. R. Forster, L. Brucker, Initial in situ measurements of perennial meltwater storage in the Greenland firn aquifer, Geophysical Research Letters 41 (2014) 81–85.

[33] C. Polashenski, Z. Courville, C. Benson, A. Wagner, J. Chen, G. Wong, R. Hawley, D. Hall, Observations of pronounced Greenland ice sheet firn

warming and implications for runoff production, Geophysical Research Letters 41 (2014) 4238–4246.

[34] A. Heilig, O. Eisen, M. MacFerrin, M. Tedesco, X. Fettweis, Seasonal monitoring of melt and accumulation within the deep percolation zone of the Greenland Ice Sheet and comparison with simulations of regional climate modeling, Cryosphere 12 (2018) 1851–1866.

[35] S. R. Ligtenberg, M. M. Helsen, M. R. Van Den Broeke, An improved semi-empirical model for the densification of Antarctic firn, Cryosphere 5 (2011) 809–819.

[36] C. T. Van Dalum, W. Jan Van De Berg, S. Lhermitte, M. R. Van Den Broeke, Evaluation of a new snow albedo scheme for the greenland ice sheet in the regional atmospheric climate model (racmo2), Cryosphere 14 (2020) 3645–3662.

[37] C. R. Steger, C. H. Reijmer, M. R. van den Broeke, N. Wever, R. R. Forster, L. S. Koenig, P. K. Munneke, M. Lehning, S. Lhermitte, S. R. Ligtenberg, C. Miège, B. P. Noël, Firn meltwater retention on the greenland ice sheet: A model comparison, Frontiers in Earth Science 5 (2017).

[38] J. M. Van Wessem, C. R. Steger, N. Wever, M. R. Van Den Broeke, An exploratory modelling study of perennial firn aquifers in the Antarctic Peninsula for the period 1979-2016, Cryosphere 15 (2021) 695–714.

[39] E. Keenan, N. Wever, M. Dattler, J. T. Lenaerts, B. Medley, P. Kuipers Munneke, C. Reijmer, Physics-based SNOWPACK model improves representation of near-surface Antarctic snow and firn density, Cryosphere 15 (2021) 1065–1085.

[40] R. S. Fausto, J. E. Box, B. Vandecrux, D. van As, K. Steffen, M. J. Macferrin, H. Machguth, W. Colgan, L. S. Koenig, D. McGrath, C. Charalampidis, R. J. Braithwaite, A snow density dataset for improving surface boundary conditions in Greenland ice sheet firn modeling, Frontiers in Earth Science 6 (2018).

[41] P. Kuipers Munneke, S. R. Ligtenberg, E. A. Suder, M. R. Van Den Broeke, A model study of the response of dry and wet firn to climate change, Annals of Glaciology 56 (2015) 1–8.

[42] R. J. Arthern, D. G. Vaughan, A. M. Rankin, R. Mulvaney, E. R. Thomas, In situ measurements of Antarctic snow compaction compared with predictions of models, Journal of Geophysical Research: Earth Surface 115 (2010) 1–12.

[43] K. Cuffey, W. Paterson, The physics of glaciers, Journal of Glaciology 57 (2011) 383–384.

[44] A. N. Horlings, K. Christianson, N. Holschuh, C. M. Stevens, E. D. Waddington, Effect of horizontal divergence on estimates of firn-air content, Journal of Glaciology 67 (2021) 287–296.

[45] B. Noël, W. J. Van De Berg, E. Van Meijgaard, P. Kuipers Munneke, R. S. Van De Wal, M. R. Van Den Broeke, Evaluation of the updated regional climate model RACMO2.3: Summer snowfall impact on the Greenland Ice Sheet, Cryosphere 9 (2015) 1831–1844.

[46] G. D. Q. Robin, Seismic shooting and related investigations: Norwegian-British-Swedish Antarctic Expedition,1949–1952, Scientific Results 5 (1958).

[47] M. M. Herron, C. C. Langway, Firn densification: an empirical model., Journal of Glaciology 25 (1980) 373–385.

[48] M. Van Den Broeke, P. Smeets, J. Ettema, C. Van Der Veen, R. Van De Wal, J. Oerlemans, Partitioning of melt energy and meltwater fluxes in the ablation zone of the west Greenland ice sheet, Cryosphere 2 (2008) 179–189.

[49] M. M. Helsen, M. R. Van Den Broeke, R. S. Van De Wal, W. J. Van De Berg, E. Van Meijgaard, C. H. Davis, Y. Li, I. Goodwin, Elevation changes in antarctica mainly determined by accumulation variability, Science 320 (2008) 1626–1629.

[50] E. E. a. Anderson, A point energy and mass balance model of a snow cover, volume 114, 1976. URL: `http://www.csa.com/partners/viewrecord.php?requester=gs&collection=ENV&recid=7`

[51] N. Calonne, L. Milliancourt, A. Burr, A. Philip, C. L. Martin, F. Flin, C. Geindreau, Thermal Conductivity of Snow, Firn, and Porous Ice

From 3-D Image-Based Computations, Geophysical Research Letters 46 (2019) 13079–13089.

[52] R. C. Reid, T. K. Sherwood, R. E. Street, The Properties of Gases and Liquids, Physics Today 12 (1959) 38–40.

[53] J. Magnusson, N. Wever, R. Essery, N. Helbig, A. Winstral, T. Jonas, Evaluating snow models with varying process representations for hydrological applications, Water Resources Research 51 (2015) 2707–2723.

[54] C. Coléou, B. Lesaffre, Irreducible water saturation in snow: experimental results in a cold laboratory, Annals of Glaciology 26 (1998) 64–68.

[55] M. Van Den Broeke, J. Bamber, J. Ettema, E. Rignot, E. Schrama, W. J. D. Van Berg, E. Van Meijgaard, I. Velicogna, B. Wouters, Partitioning recent Greenland mass loss, Science 326 (2009) 984–986.

[56] E. M. Enderlin, I. M. Howat, S. Jeong, M.-J. Noh, J. H. Van Angelen, M. R. Van Den Broeke, An improved mass budget for the Greenland ice sheet, Geophysical Prospecting (2014) 6413–6419.

[57] M. McMillan, A. Leeson, A. Shepherd, K. Briggs, T. W. Armitage, A. Hogg, P. Kuipers Munneke, M. van den Broeke, B. Noël, W. J. van de Berg, S. Ligtenberg, M. Horwath, A. Groh, A. Muir, L. Gilbert, A high-resolution record of Greenland mass balance, Geophysical Research Letters 43 (2016) 7002–7010.

[58] J. Harper, N. Humphrey, W. T. Pfeffer, J. Brown, X. Fettweis, Greenland ice-sheet contribution to sea-level rise buffered by meltwater storage in firn - supplementary material, Nature 491 (2012) 240–243.

[59] A. Heilig, O. Eisen, M. Schneebeli, M. MacFerrin, C. M. Stevens, B. Vandecrux, K. Steffen, Relating regional and point measurements of accumulation in southwest Greenland, The Cryosphere 14 (2020) 385–402.

[60] R. R. Forster, J. E. Box, M. R. Van Den Broeke, C. Miège, E. W. Burgess, J. H. Van Angelen, J. T. Lenaerts, L. S. Koenig, J. Paden, C. Lewis, S. P. Gogineni, C. Leuschen, J. R. McConnell, Extensive liquid meltwater storage in firn within the Greenland ice sheet, Nature Geoscience 7 (2014) 95–98.